INTERFACE SCIENCE 10, 149–158, 2002

Atomic-Scale Simulation Study of Equilibrium Solute Adsorption at Alloy Solid-Liquid Interfaces

H. RAMALINGAM, M. ASTA AND A. VAN DE WALLE
Department of Materials Science and Engineering, Northwestern University, Evanston, IL 60081, USA

J.J. HOYT
Sandia National Laboratories, Albuquerque, NM 87185, USA

Abstract. Equilibrium structural properties of solid-liquid interfaces in Cu-Ni alloys are studied by Monte-Carlo simulations employing interatomic potentials based on the embedded-atom method. We describe a thermodynamic-integration approach used to derive bulk concentrations and densities for solid and liquid phases in two-phase thermodynamic equilibrium. These results are used as a basis for constructing three-dimensional supercell geometries employed in Monte-Carlo-simulation studies of solid-liquid interface properties for {100} and {111} crystallographic orientations. At a temperature of 1750 K (four percent below the calculated melting point of pure Ni) equilibrium density and concentration profiles have been derived, allowing a calculation of the relative Gibbsian adsorption, $\Gamma_{\mathrm{Cu}}^{(\mathrm{Ni})}$, of Cu (solute) relative to Ni (solvent) at solid-liquid interfaces in Ni-rich alloys. We derive absorption values of $\Gamma_{\mathrm{Cu}}^{(\mathrm{Ni})} = -0.05 \pm 0.20$ and -0.23 ± 0.50 atoms/nm^2 for {100} and {111} interfaces, respectively. These results are discussed in the context of available experimental measurements and continuum-theory results for adsorption at heterophase interfaces.

Keywords: solid-liquid interface, Monte-Carlo simulations, interface adsorption

1. Introduction

Atomic-scale computer simulations continue to play a critical role in the development of a microscopic theoretical understanding of the properties of solid-liquid interfaces. The substantial challenges associated with experimentally characterizing these properties has led to extensive simulation work over the past twenty years devoted to analysis of structure, thermodynamics and kinetic processes at solid-liquid interfaces in elemental systems. This work has included detailed investigations of density and diffusion profiles (see [1–3], and references cited therein) and growth kinetics [3–12] in systems governed by hard-sphere, pair-wise and many-body interatomic potentials. The determination of the solid-liquid interfacial free energies from atomic-scale simulations has proven to be a significant challenge. To date only five calculations of solid-liquid interfacial free energies have been published, by Broughton and Gilmer [13] for a Lennard-Jones system, Davidchack and Laird [14] for hard-spheres, Hoyt et al. [15] and Morris et al. [16] for elemental Ni and Al, respectively, as modeled through embedded-atom-method (EAM) [17] potentials, and Ravelo and Baskes for the interface between solid Cu and liquid Sn [18].

Despite the technological importance of alloys far fewer simulation studies have been devoted to the properties of solid-liquid interfaces in mixtures [19–24]. A detailed analysis of crystallization kinetics in Lennard-Jones mixtures was performed through Monte-Carlo (MC) simulations by Huitema et al. [19] who studied the transition from smooth to rough growth as a function of solute-solvent interaction strength and temperature. Yu et al. [20], and more recently Celestini and Debierre [21], used molecular-dynamics (MD) simulations to study non-equilibrium partitioning and the phenomenon of solute trapping in Si-Ge and Lennard-Jones alloys. MD has been used also to characterize

the structure and diffusion profiles at interfaces between coexisting solid and liquid alloy phases in hard-sphere [22, 23] and model-ionic [24] systems. Davidchack and Laird [23] performed a detailed analysis of density and diffusion profiles across {100} and {111} disordered face-centered cubic crystal/melt interfaces for a mixture of hard spheres with a diameter ratio equal to 0.9. The analysis of the density profiles led to an important conclusion that equilibrium segregation to the solid-liquid interface is minimal in this system.

In the present paper we describe the application of Monte-Carlo simulations to the study of solid-liquid interface structure in alloys. Equilibrium properties of {100} and {111} solid-liquid interfaces are calculated in the Cu-Ni alloy system, modeled by EAM interatomic potentials [17, 25]. The MC method is used as the basis for studying the equilibrium solute segregation to solid-liquid interfaces in this system. Specifically, we focus on calculating the magnitude and anisotropy of the relative adsorption coefficient ($\Gamma_1^{(2)}$) defined as the excess number of solute atoms (species 1) if the Gibbs dividing surface is chosen so that the excess of solvent (species 2) is zero (see, e.g., Ref. [26]). This quantity (which is independent of the positioning of the dividing surface) is equal to the negative of the partial derivative of the interfacial free energy with respect to the chemical potential of the solute species at constant temperature and pressure. Hence, appreciable adsorption affects both the thermodynamic and kinetic properties of the solid-liquid interface. Furthermore, since adsorption may depend appreciably upon the crystallographic orientation of the interface, it provides a source of anisotropy in the properties of the solid-liquid interface. The microstructure morphology resulting from dendritic solidification is critically influenced by the degree of anisotropy in solid-liquid interfacial free energies and mobilities. Hence, a knowledge of the magnitude and anisotropy of equilibrium segregation to solid-liquid interfaces is important for quantitative modeling of solidification-microstructure evolution in alloys.

2. Simulation Method and Results

Monte-Carlo simulations have been employed to study the equilibrium structure, thermodynamic properties and adsorption at solid-liquid interfaces in Cu-Ni alloys. Cu-Ni was chosen as a prototypical metallic system with small size mismatch and nearly ideal solution thermodynamic properties (see below). The energetics of Cu-Ni alloys were modeled by EAM [17] potentials, developed by Foiles [25], that have been employed in previous simulation studies of alloy thermodynamic properties [27] as well as solute segregation to surfaces [17], grain boundaries [28, 29] and dislocation cores [29, 30]. As will be described below, the simulated solid-liquid phase boundaries derived from these potentials show discrepancies with experimental measurements; the results of the present study therefore should be viewed as being representative of a prototypical metallic alloy with nearly ideal solution thermodynamic properties, rather than as quantitative predictions for the real Cu-Ni system.

Simulations of solid-liquid interfaces were performed using three-dimensional supercell geometries such as the one shown in cross-section in Fig. 1. In the present section we detail the Monte-Carlo simulation approach used to equilibrate and characterize equilibrium density and composition profiles across solid-liquid interfaces. Results for equilibrium solid-liquid interface structural properties, and the relative interfacial adsorption of Cu solute atoms in Ni-rich alloys are presented for {100} and {111} crystallographic orientations.

2.1. *Solid-Liquid Phase Boundaries*

A simulation study of the equilibrium properties of an alloy solid-liquid interface requires knowledge of the bulk composition-temperature phase diagram. Specifically, for a given temperature (T) and pressure (P), values of the composition and density are required for each of the solid and liquid phases under conditions of two-phase thermodynamic equilibrium. To determine the solidus and liquidus phase boundaries, we employed Monte-Carlo simulations, coupled with thermodynamic-integration calculations of Gibbs free energies as a function of alloy concentration.

In the thermodynamic-integration calculations, we begin by deriving the difference in chemical potentials $\mu_{\mathrm{Ni}}^{\mathrm{s}}$ and $\mu_{\mathrm{Ni}}^{\mathrm{l}}$ of the pure solvent (Ni in the present study) in the solid and liquid phases, respectively, as a function of temperature. These values serve as reference points for the integration of Gibbs free energies as a function of solute composition (Cu in this work) at constant temperature (see Eq. (3) below). For pure Ni we employ the following thermodynamic relation between the chemical potential and the enthalpy per

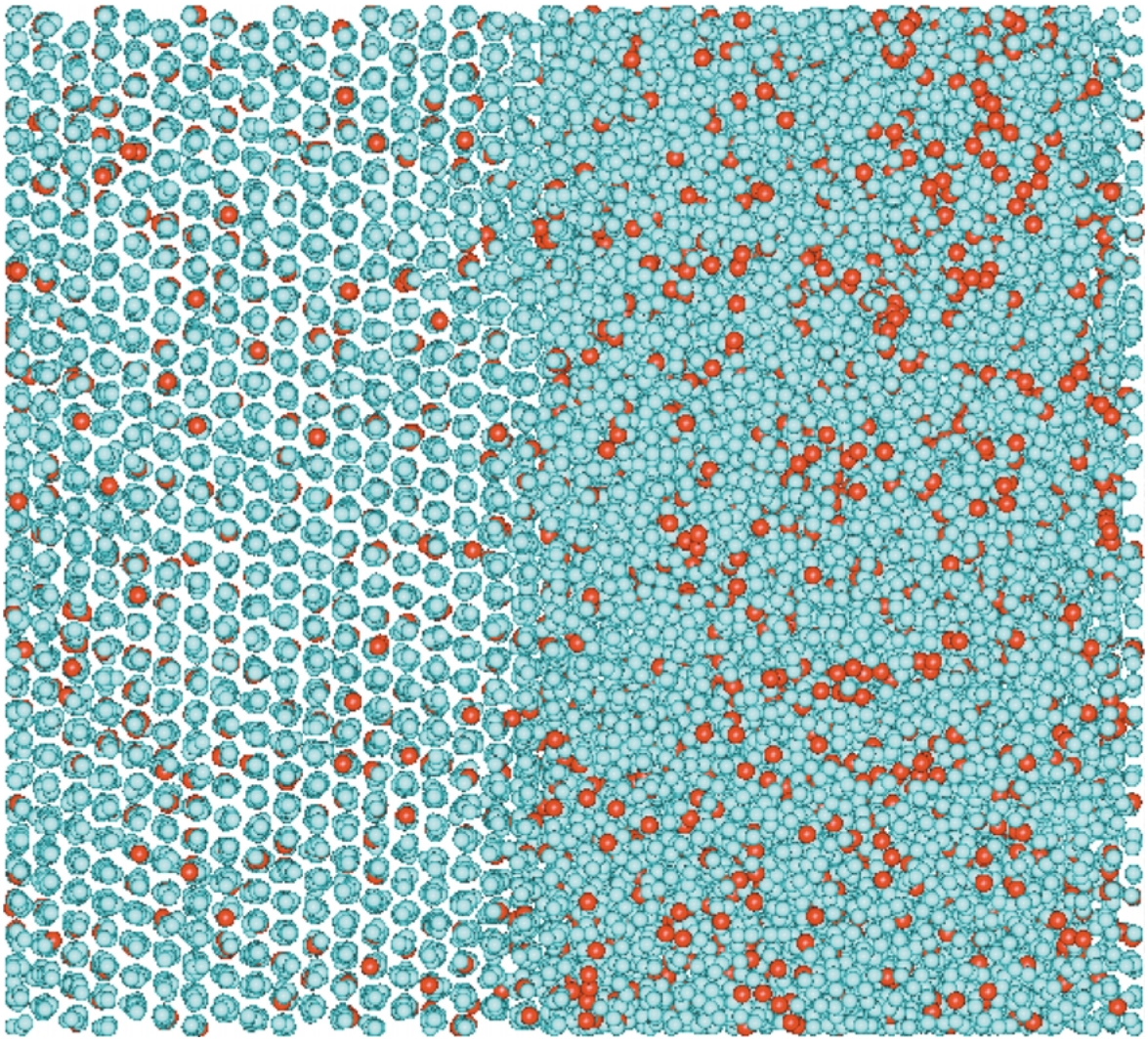

Figure 1. Snapshot of a Monte-Carlo simulation for a {111} solid-liquid interface in Cu-Ni. Blue and red circles represent Ni and Cu atoms, respectively.

atom (H):

$$\left(\frac{\partial(\mu/T)}{\partial T}\right)_P = -\frac{1}{T^2}H \qquad (1)$$

which can be integrated from the melting point (where the chemical potentials of Ni in the solid and liquid phases are equal) to determine $\mu^s - \mu^l$ as a function of temperature:

$$\frac{\mu^s - \mu^l}{T} = \int_T^{T_m} \frac{H^s(T') - H^l(T')}{T'^2}\, dT' \qquad (2)$$

The application of Eq. (2) requires the knowledge of melting temperature (T_m), as well as the values of H^s and H^l as a function of temperature.

The melting point of pure Ni was obtained as follows. Half of the atoms in an 8000-atom ($10 \times 10 \times 20$ fcc unit cells) simulation cell were melted at a high temperature much above the experimental melting point, producing a non-equilibrium {100} solid-liquid interface structure. Subsequently, the entire structure was allowed to evolve in Monte-Carlo simulations at different temperatures near the estimated value of T_m. These simulations made use of the Metropolis algorithm, sampling over displacive degrees of freedom

(by attempting random displacements with a maximum value of 0.1 for each coordinate), and allowing the periodic lengths of the Monte-Carlo cell to evolve to maintain zero stress. For temperatures above the melting point the liquid portion of the cell grows at the expense of the crystalline portion, while below T_m the structure solidifies. By monitoring the evolution of the structure, volume and energy during such simulations the melting point was bracketed and estimated to be around 1820 K.

Subsequently, the solid-liquid interface structure employed in the Monte-Carlo simulations was used the basis for Molecular-Dynamics (MD) simulations of phase coexistence along the lines described by Morris et al. [31]. These MD simulations were performed in the microcanonical ensemble (fixed particle number, volume and energy) and the equilibrium melting point was derived from the average temperature and pressure obtained during a 2 nanosecond simulation for the two-phase solid-liquid system. During these simulations the length of the simulation box in the directions parallel to the interface were fixed by the equilibrium (zero pressure) lattice constant calculated for bulk Ni at 1820 K. The length of the box perpendicular to the interface was adjusted to minimize as much as possible the stress normal to the interfaces in the system. In these simulations the temperature, normal stress, and the so-called "crystal stress" [2] in the solid were monitored. The crystal stress is defined as $\sigma_c = \sigma_{zz} - (\sigma_{xx} + \sigma_{yy})/2$, where σ_{ij} denotes the (i, j) component of the stress tensor, x and y are directions parallel to the solid-liquid interface while z is normal. We obtained an average temperature of $T = 1819 \pm 2$ K, while the average stresses were $\sigma_{zz} = -244 \pm 400$ Bars and $\sigma_c = -200 \pm 800$ Bars (all error estimates reported in this paper correspond to 95 percent confidence levels). From the calculated average temperature and stresses the Clausius-Clapeyron relation was used to estimate a zero-pressure value of the melting point equal to $T_m = 1820 \pm 6$ K for Ni, based on EAM potential of Foiles [25] (i.e., the stress levels in the solid-liquid interface simulation were sufficiently small to produce a relatively small correction to the melting point). This result is to be compared with the experimentally measured value of 1728 K.

Experimentally, the solidus and liquidus phase boundaries for Cu-Ni are of a single "lens" type, characteristic of nearly ideal solutions [32]. The simulations for solid-liquid interfaces in this study were performed at 1750 K, which is roughly four percent below the calculated melting point of pure Ni. Enthalpy versus temperature data for pure Ni, required for the evaluation of Eq. (2), were derived from 4000-atom Monte-Carlo simulations for both liquid and solid phases. Simulations were performed at 10 K temperature intervals between 1820 and 1750 K sampling over the displacive degrees of freedom, as described above, for a total 5×10^4 Monte-Carlo steps/atom (MCS) at each temperature (note that the liquid phase was metastable over this temperature range).

With the above values for the chemical potentials of pure Ni, the Gibbs free energy is calculated as a function of Cu concentration (X_{Cu}) from a separate thermodynamic integration approach using the following relation:

$$\left(\frac{\partial G}{\partial X_{\mathrm{Cu}}}\right)_{P,T} = \Delta\mu(X_{\mathrm{Cu}}, P, T) \tag{3}$$

where G is the Gibbs free energy per atom in the alloy, and $\Delta\mu = \mu_{\mathrm{Ni}} - \mu_{\mathrm{Cu}}$ is the chemical potential difference between Ni and Cu in a given phase (solid or liquid). Monte-Carlo simulations in the so-called semi-Grand-Canonical ensemble (also referred to as the Transmutation ensemble, see, e.g., [33]) are performed to calculate the relation between the imposed $\Delta\mu$ and the ensemble average $\langle X_{\mathrm{Cu}} \rangle$. In these simulations the total number of atoms remains fixed but the relative concentration of each chemical species is allowed to evolve in response to an externally imposed chemical potential difference $\Delta\mu$. For the purposes of integrating Eq. (3) the calculated $\Delta\mu$ vs. $\langle X_{\mathrm{Cu}} \rangle$ results are fit to the following functional form:

$$\Delta\mu(X_{\mathrm{Cu}}, P, T) = k_B T \ln\left(\frac{X_{\mathrm{Cu}}}{1 - X_{\mathrm{Cu}}}\right) + \sum_{i=0}^{n} A_i X_{\mathrm{Cu}}^i \tag{4}$$

where the first and second terms on the right-hand side correspond to ideal and non-ideal contributions to $\Delta\mu$, respectively. Once the parameters A_i have been derived by fitting to zero-pressure Monte-Carlo data, Eq. (4) is used to integrate Eq. (3) giving a formula for G as a function of concentration:

$$\begin{aligned} G(T, X_{\mathrm{Cu}}) = {} & G(T, X_{\mathrm{Cu}} = 0) + k_B T [X_{\mathrm{Cu}} \ln X_{\mathrm{Cu}} \\ & + (1 - X_{\mathrm{Cu}}) \ln(1 - X_{\mathrm{Cu}})] \\ & + \sum_{i=0}^{n} A_i X_{\mathrm{Cu}}^{i+1} / (i + 1) \end{aligned} \tag{5}$$

In Eq. (5), the first term on the right-hand-side is the chemical potential of pure Ni (μ_{Ni}), the second is

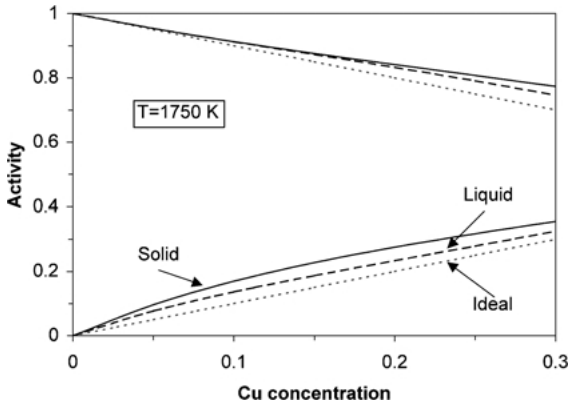

Figure 2. Activity coefficients for Cu and Ni in solid and liquid phases at 1750 K derived from Monte-Carlo thermodynamic integration.

the ideal mixing free energy, and the third represents the excess contributions to G. For the purpose of deriving phase boundaries we take $\mu^{s}_{Ni} = 0$ in the solid phase, and μ^{l}_{Ni} is given by the value of $\mu^{s}_{Ni} - \mu^{l}_{Ni}$ quoted above.

The semi-Grand-Canonical Monte-Carlo simulations were performed with a fixed total number of 4000 atoms, for a range of imposed chemical potential differences $\Delta\mu$ at $T = 1750$ K. Monte-Carlo sampling was performed over displacive and cell-size (to maintain zero pressure) degrees of freedom as described above, and in addition, changes in chemical identity were attempted on average once every other MCS during simulations lasting 5×10^4 MCS for each value of $\Delta\mu$. A result of such simulations is the average composition $\langle X_{Cu} \rangle$ versus the imposed chemical potential difference $\Delta\mu$ at zero pressure. For both solid and liquid phases this data was accurately fit by Eq. (4) with a second-order polynomial over the concentration range between zero and thirty atomic percent Cu. Free energy results obtained by integrating Eq. (5) are shown in Fig. 2, plotted in the form of activity coefficients (a_{Cu}, a_{Ni}) versus X_{Cu}. The dotted lines correspond to ideal solutions ($a_{Cu} = X_{Cu}$, $a_{Ni} = X_{Ni}$), and a comparison with the EAM-Monte-Carlo results demonstrates a weak positive deviation from ideal solution thermodynamics for both solid and liquid phases. This tendency is consistent with the presence of a low-temperature miscibility gap in the Cu-Ni system (observed experimentally [32] and predicted by the EAM potentials [27]) and is in qualitative agreement with measurements [34].

From the calculated free energy curves for solid and liquid phases, the equilibrium phase boundaries are derived by the usual common-tangent construction. The resulting solidus and liquidus compositions (X^{s}_{Cu}, X^{l}_{Cu}) at $T = 1750$ K are listed in the first row of Table 1. The quoted errors are estimated based on the uncertainties in (i) the chemical potentials of pure Ni (see above) as well as (ii) the values of $\langle X_{Cu} \rangle$ versus $\Delta\mu$ derived from the semi-Grand-Canonical Monte-Carlo simulations. The EAM potentials give rise to a predicted value for the equilibrium partition coefficient, X^{s}_{Cu}/X^{l}_{Cu}, equal to 0.5 at 1750 K. Experimentally, at the temperature of 1642 K (corresponding to 95 percent of the melting point of pure Ni, as in the simulations) this ratio is measured to be roughly 0.6 [32].

As detailed further in the next section, to set up a simulation cell for the study of equilibrium properties of solid-liquid interfaces, the densities of the bulk solid and liquid phases are required at the equilibrium solidus and liquidus compositions. These values are listed in the first row of Table 1, derived from Monte-Carlo simulations for 4000-atom cells at 1750 K.

2.2. *Solid-Liquid Interface Simulations*

Monte-Carlo simulations were used to study the equilibrium structural properties of solid-liquid interfaces with (100) and (111) crystallographic orientations at $T = 1750$ K. As in the previous section we refer to the direction perpendicular to the interface as the z axis. In the x-y plane, the lengths of the cells were dictated by the lattice constant of the crystalline phase,

Table 1. For solid and liquid phases in thermodynamic equilibrium at 1750 K: The mole fractions of Cu in the solid (X^{s}_{Cu}) and liquid (X^{l}_{Cu}) phases, and the atomic densities of Ni and Cu.

	X^{s}_{Cu} (at.%)	X^{l}_{Cu} (at.%)	Solid density (nm^{-3})	Liquid density (nm^{-3})	$\Gamma^{(Ni)}_{Cu}$ (nm^{-2})
Bulk	5.0 ± 0.4	10.1 ± 0.4	83.2 ± 0.1	77.1 ± 0.1	–
{100}	4.86 ± 0.05	11.0 ± 0.1	83.3 ± 0.3	76.2 ± 0.3	-0.05 ± 0.20
{111}	4.94 ± 0.05	10.4 ± 0.1	83.4 ± 0.2	76.8 ± 0.2	-0.23 ± 0.50

$\Gamma^{(Ni)}_{Cu}$ denotes the relative adsorption of Cu relative to Ni.

determined from the bulk density given in Table 1, which corresponds to a lattice parameter for the fcc solid-solution phase of 3.636 Å at $T = 1750$ K. The total number of atoms in the simulation cells was 16000 for (100) and 16128 for (111), set up with 80 crystalline planes normal to the z direction for (100) and 72 for (111). In-plane dimensions were 36.360×36.360 for (100) and 35.995×35.625 along the [110] and [$11\bar{2}$] directions, respectively, for (111).

Initially, half of the atoms (i.e., all atoms located in the top-half of the cell along the z-direction) in the simulation cell were melted at high temperature keeping the positions of the atoms in the bottom half of the cell fixed at ideal crystalline sites. The simulation cells then were equilibrated at $T = 1750$ K. During the equilibration of solid-liquid interface structures the z-lengths of the simulation cells were adjusted to minimize the σ_{zz}. Density and composition profiles were equilibrated through Monte-Carlo sampling in the semi-Grand-canonical ensemble (see previous section) involving attempted atomic displacements and changes in chemical identity with an imposed chemical potential difference $\Delta\mu$ derived from the bulk phase-boundary calculations described above. Equilibration was gauged by monitoring the evolution of the stress and densities in the solid and liquid phases.

Subsequent to the equilibration of the solid-liquid interface cells simulations were performed to characterize the equilibrium concentration and density profiles, following an approach similar to that employed by Davidchack and Laird [2] in detailed studies of hard-sphere systems. The approach relies upon a reliable method for tracking the average position of the interface through the simulation. For this purpose we made use of a structural order parameter introduced by Hoyt et al. [15]. The order parameter for a given atom i is defined as follows:

$$\eta_i = \frac{1}{12} \sum_{j=1}^{12} \left| r_j - r_j^{\text{ideal}} \right|^2 \tag{6}$$

where the sum is over the 12 nearest neighbors of i, r_j is the instantaneous position of neighboring atom j, and r_j^{ideal} is the corresponding "ideal" position of a neighboring atom site in a perfect fcc crystal. By performing averages of the values of η over atoms within slices normal to z, instantaneous order-parameter profiles are calculated. The planar-averaged order parameter varies between values of roughly $0.2^{\,2}$ in the crystalline phase to $1.2^{\,2}$ in the liquid. The instantaneous position of interface along z is defined by a value for the order parameter equal to $0.875^{\,2}$.

Density profiles were calculated by averaging the number of atoms within small volume elements normal to the z-axis:

$$\rho(z) = \frac{\langle N(z) \rangle}{A \Delta_z} \tag{7}$$

where $N(z)$ is the number of particles in a slice of width Δ_z centered at z, and A is the cross-sectional area. The width of the slices was chosen to be $L_z/3600$ for both (100) and (111) cells (corresponding to roughly 45 slices per crystallographic plane), where L_z is the periodic length normal to the interfaces. In both MD and MC simulations of solid-liquid interface structures it has been found that the average position of the crystalline portion of the simulation cell fluctuates due to Brownian motion [2]. Consequently, for the purpose of averaging density profiles the coordinate z in Eq. (7) was referenced to the instantaneous averaged position of the atoms in the crystalline portion of the cell. Instantaneous density profiles and interface positions (derived from the structural order parameter defined above) were stored once every 100 MCS during Monte-Carlo sampling runs lastly roughly 5×10^5 MCS for each interface orientation. Subsequently, density profiles were averaged over a few hundred configurations for which the interface positions differed by less than half of the crystalline interplanar spacing. The resulting averaged density profiles in the vicinity of the solid-liquid interfaces are plotted in Fig. 3(a) and (b). In these figures the solid and dashed lines correspond to the densities of Ni (solvent) and Cu (solute) atoms, respectively, and the zero of the z-coordinate corresponds to the average position of the interface as derived from the structural order-parameter described above. In Fig. 3 the solid region is clearly identified on the left-hand-side of the interface by the oscillations in the density profiles characteristic of crystalline long-range order. These oscillations dampen out across the interface over a distance of roughly a nanometer, and the average density becomes uniform in the liquid phase.

In Fig. 4 we plot average concentration profiles derived from the MC sampling simulations described above. In this figure, each data point corresponds to the average concentration of Cu atoms within a "coarse" bin of width Δz, equal to the average bulk interplanar spacing for each interface orientation. The averaging was performed over 1000 density

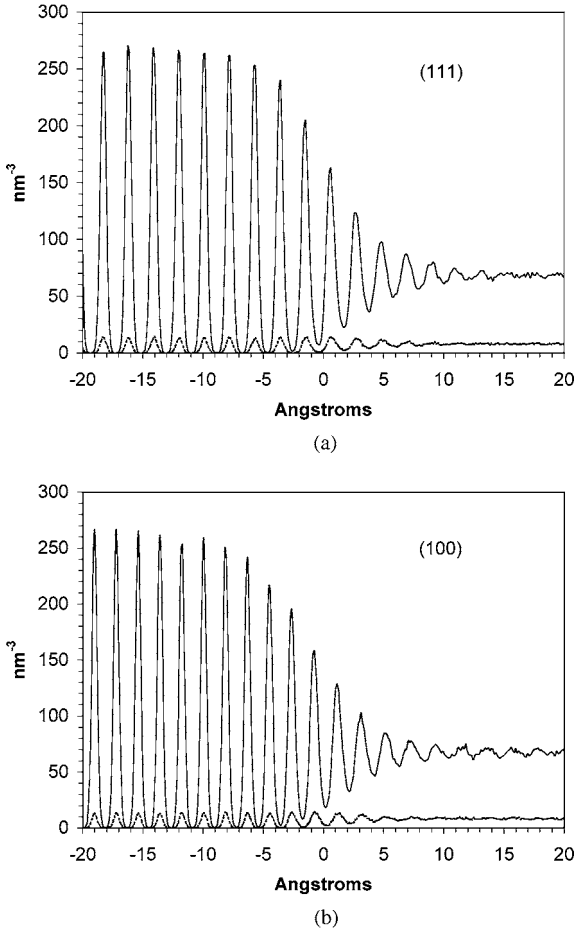

Figure 3. Density profiles for (a) {111} and (b) {100} solid-liquid interfaces in Cu-Ni derived from Monte-Carlo simulation. Solid and dashed lines represent density profiles for Ni (solvent) and Cu (solute), respectively.

profiles stored during the sampling MC runs, and for each configuration the boundaries of the averaging bins were adjusted relative to the instantaneous interface positions. The solid-lines in Fig. 4 give the best fit of the MC-concentration profile data to the function $X_{\mathrm{Cu}}(z) = \bar{X}_{\mathrm{Cu}} + \Delta X_{\mathrm{Cu}} \tanh[(z - z_0)/w]$ where $\bar{X}_{\mathrm{Cu}} = (X^{\mathrm{l}}_{\mathrm{Cu}} + X^{\mathrm{s}}_{\mathrm{Cu}})/2$ represents the average of the bulk solid and liquid Cu concentrations, $\Delta X_{\mathrm{Cu}} = (X^{\mathrm{l}}_{\mathrm{Cu}} - X^{\mathrm{s}}_{\mathrm{Cu}})/2$ is the difference in Cu concentrations between the bulk phases, z_0 corresponds to the center of the concentration profile, and w is related to the profile width. The best fit to the Monte-Carlo data gives a value of w equal to 3.3 ± 0.4 Å for both (100) and (111) orientations, corresponding to a "10–90" interface widths of 7.2 ± 0.9 Å.

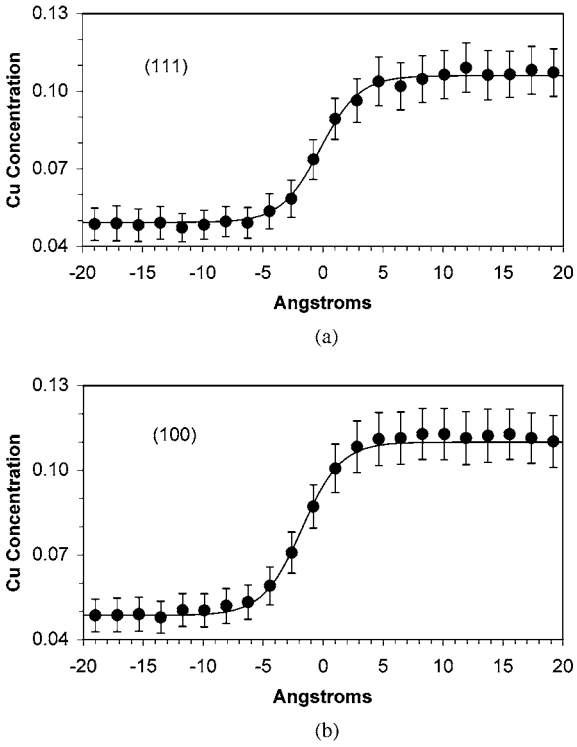

Figure 4. Monte-Carlo-calculated composition profiles for (a) {111} and (b) {100} solid-liquid interfaces in Cu-Ni.

2.3. *Adsorption Coefficient*

The Monte-Carlo simulation procedure described in the previous sections was also employed to derive the relative Gibbsian adsorption of Cu solute to the solid-liquid interface in Ni-rich alloys at $T = 1750$ K. The excess of Cu (solute) relative to Ni (solvent), is defined by the equation (see, e.g., [26]):

$$\Gamma^{(\mathrm{Ni})}_{\mathrm{Cu}} = \Gamma_{\mathrm{Cu}} - \Gamma_{\mathrm{Ni}}\left(\rho^{\mathrm{l}}_{\mathrm{Cu}} - \rho^{\mathrm{s}}_{\mathrm{Cu}}\right)\Big/\left(\rho^{\mathrm{l}}_{\mathrm{Ni}} - \rho^{\mathrm{s}}_{\mathrm{Ni}}\right) \qquad (8)$$

where $\rho^{\mathrm{l}}_{\mathrm{Ni}}$ and $\rho^{\mathrm{s}}_{\mathrm{Ni}}$ are the densities of Ni atoms in the bulk liquid and solid, respectively, and similarly for $\rho^{\mathrm{l}}_{\mathrm{Cu}}$ and $\rho^{\mathrm{s}}_{\mathrm{Cu}}$. Γ_{Ni} and Γ_{Cu} are the adsorption coefficients for Ni and Cu, respectively, obtained with an arbitrarily chosen dividing surface. In a periodic supercell with fixed periodic lengths, the adsorption coefficient of Ni can be written in the following form:

$$2A\Gamma_{\mathrm{Ni}} = N_{\mathrm{Ni}} - AL^{\mathrm{s}}\rho^{\mathrm{s}}_{\mathrm{Ni}} - AL^{\mathrm{l}}\rho^{\mathrm{l}}_{\mathrm{Ni}} \qquad (9)$$

where N_{Ni} is the total number of Ni atoms in the simulation cell, A is the cross-sectional area, L^{l} is the length

of the liquid region between the Gibbs dividing surfaces for the two interfaces, and $L^s = L_z - L^l$ is the length of the solid region, where as above L_z is the total periodic length of the simulation cell normal to the interface. The factor of 2 in Eq. (9) accounts for the presence of two interfaces in the periodic cell. A similar relation can be written for Γ_{Cu}. When these formulas for Γ_{Ni} and Γ_{Cu} are inserted into Eq. (8), an expression for $\Gamma_{Cu}^{(Ni)}$ is obtained that is a function of L_z, the bulk densities of Cu and Ni in each phase, and the average number of solute and solvent atoms in the simulation cell:

$$2A\Gamma_{Cu}^{(Ni)} = N_{Cu} - AL_z\left[\rho_{Cu}^s - \rho_{Ni}^s \frac{\rho_{Cu}^l - \rho_{Cu}^s}{\rho_{Ni}^l - \rho_{Ni}^s}\right] - N_{Ni}\frac{\rho_{Cu}^l - \rho_{Cu}^s}{\rho_{Ni}^l - \rho_{Ni}^s} \quad (10)$$

It is worth emphasizing that although the absolute values of the adsorption coefficients Γ_{Ni} and Γ_{Cu} (see Eq. (9)) depend on the location of the Gibbs dividing surface, the relative adsorption defined in Eq. (10) is invariant with respect to these positions.

From Eq. (10) the calculation of $\Gamma_{Cu}^{(Ni)}$ reduces to determining the densities of Cu and Ni in the bulk solid and liquid portion of the supercell (away from the interfacial regions), as well as the average values of N_{Ni} and N_{Cu}. The required bulk densities were extracted from the interface simulations rather than from the previously described bulk calculations, in order to minimize the effect of systematic sources of error in the estimated density profiles. As will be discussed below, a source of systematic error in comparing bulk and solid-liquid-interface results is differences in the states of stress associated with the different simulation geometries. To calculate these density values in a manner that reduces statistical uncertainties as much as possible, we made use of "averaging windows" by identifying regions along z in the solid and liquid portions of the simulation cells where the average density and concentration is uniform (away from the interface regions). Bulk densities were derived by averaging the number of atoms of each type within these bulk "averaging window" regions, sampled once every 100 MCS during Monte-Carlo simulations run for a total length of roughly 10^5 steps. To reduce noise in the sampling, the boundaries of the averaging windows were defined relative to the instantaneous position of the atoms in the crystalline region (to account for Brownian motion of the crystal as described above) and the width of the window in the solid phase was taken commensurate with the average interplanar spacing.

The average bulk densities and Cu concentrations derived from the solid-liquid interface simulation cells, along with their associated statistical uncertainties, are listed in Table 1. Small, yet statistically significant, discrepancies are noted between the numbers for the liquid-phase properties obtained in the two different interface simulation cells, as well as in the bulk simulations described in Section 2.1. These discrepancies can be accounted for based on the differences in the averaged stress states for each simulation. Specifically, in the solid-liquid interface simulations the periodic lengths normal to the interface were taken as 150.994 for (100) and 156.839 for (111). With these fixed lengths, the average stress normal to the interface was small but non-zero, amounting to $\sigma_{zz} = -1600 \pm 1100$ and $\sigma_{zz} = -300 \pm 900$ Bars for (100) and (111) interface cells, respectively. Additionally, the crystal stress was monitored in the solid-portion of the cell and was calculated to be $\sigma_c = 600 \pm 400$ and $\sigma_c = 1500 \pm 1600$ Bars for (100) and (111), respectively. For the crystalline portion of the cell the average stress state was therefore non-hydrostatic with a compressive in-plane stress of roughly 2 kBar for both orientations, and tensile normal stresses of -1.6 and 0.3 kBar for cells with (100) and (111) oriented interfaces, respectively. The (hydrostatic) pressure in the liquid phase was -1.6 and 0.3 kBar for the (100) and (111) solid-liquid interface simulations. In bulk semi-Grand-canonical MC simulations at fixed $\Delta\mu$, a decrease in the pressure of the liquid by 1 kBar was found to lead to a decrease in density and increase in composition of approximately 0.2 nm^{-3} and 0.2 at.%, respectively, comparable to the level of discrepancy noted between the different simulation results listed in Table 1.

When the calculated values of the bulk densities and compositions given in Table 1 are inserted into Eq. (10), the estimates of $\Gamma_{Cu}^{(Ni)}$ listed in the final column of Table 1 result. We obtain -0.05 ± 0.20 and -0.23 ± 0.60 atoms/nm^2 for the relative adsorptions at {100} and {111} interfaces, respectively. For reference, a monolayer of atoms corresponds to 15.0 and 17.3 atoms/nm^2 for {100} and {111} interfaces, respectively. Our adsorption results therefore correspond to a magnitude of the interface adsorption of no more than a few percent of a monolayer for both interface orientations. No statistically significant anisotropy in the relative adsorption is found in this work.

3. Summary and Discussion

A Monte-Carlo method for equilibrating and analyzing the structure of solid-liquid interfaces in alloys has been described. The method has been applied to the study of density and composition profiles and equilibrium segregation to solid-liquid interfaces in the binary Cu-Ni alloy system modeled using EAM interatomic potentials. Equilibrium concentration profiles are characterized by a calculated 10–90 interface width of 7.2 ± 0.9 Angstroms for both {100} and {111} orientations. The main conclusion of the work concerns the magnitude of the relative Gibbsian adsorption ($\Gamma_{\mathrm{Cu}}^{(\mathrm{Ni})}$), calculated to be -0.05 ± 0.20 and -0.23 ± 0.50 atoms/nm^2 for {100} and {111} oriented solid-liquid interfaces, respectively. Importantly, we find no statistically significant anisotropy in the interface segregation. Within the statistical uncertainties, the calculated values of $\Gamma_{\mathrm{Cu}}^{(\mathrm{Ni})}$ correspond to less than ten percent of a monolayer adsorption of Cu relative to Ni. These values are several times smaller than those measured for semicoherent heterophase interfaces in metal-alloy/ceramic systems [35, 36] and calculated for coherent interfaces between solid-phase ternary alloys [37, 38]. The relatively small values of $\Gamma_{\mathrm{Cu}}^{(\mathrm{Ni})}$ obtained in this study are consistent with the simulation results of Davidchack and Laird [23] who found no statistically significant relative adsorption to {100} and {111} solid-liquid interfaces in hard-sphere mixtures.

Our results are interesting in light of a very recent continuum theoretical analysis of Gibbsian adsorption to heterophase interfaces performed by Umantsev [39]. Umantsev calculated analytical expressions for the relative adsorptions at heterophase interfaces in multicomponent alloys within a square gradient (Cahn-Hilliard type) continuum formalism. For *linear systems*, i.e., systems in which the chemical potentials and pressure depend linearly on densities in both the solid and liquid phases, he concluded that relative Gibbsian adsorption coefficients are identically equal to zero. Importantly, however, the continuum analysis of Umantsev suggests that Gibbsian adsorption to solid-liquid interfaces need not be small in general. Specifically, adsorption may be appreciable in systems for which the linear approximation breaks down, e.g., systems with large composition and density differences between solid and liquid phases. Clearly, further work is warranted to characterize equilibrium segregation to solid-liquid interfaces more generally in a wider variety of alloys.

Acknowledgments

This research was supported by the U. S. Department of Energy, Office of Basic Energy Sciences, Materials Science Division, under contract No. DE-FG02-01ER45910, and by the Computational Materials Science Network. This work was supported in part by a Laboratory Directed Research and Development grant from Sandia National Laboratories. We acknowledge helpful discussions with David Seidman and Alex Umantsev, and the use of an EAM Monte-Carlo code developed by Stephen Foiles. We thank Prof. Brian Laird for a critical reading of the manuscript.

References

1. B.B. Laird and A.D.J. Haymet, Chem. Rev. **92**, 1819 (1992).
2. R.L. Davidchack and B.B. Laird, J. Chem. Phys. **108**, 9452 (1998).
3. H.E.A. Huitema, M.J. Vlot, and J.P. van der Eerden, J. Chem. Phys. **111**, 4714 (1999).
4. J.Q. Broughton, G.H. Gilmer, and K.A. Jackson, Phys. Rev. Lett. **49**, 1496 (1982).
5. E. Burke, J.Q. Broughton, and G.H. Gilmer, J. Chem. Phys. **89**, 1030 (1988).
6. H.E.A. Huitema and J.P. van der Eerden, J. Chem. Phys. **110**, 3267 (1999).
7. W.J. Briels and H.L. Tepper, Phys. Rev. Lett. **79**, 5074 (1997).
8. J.J. Hoyt, B. Sadigh, M. Asta, and S.M. Foiles, Acta Mater. **47**, 3181 (1999).
9. L.A. Baez and P. Clancy, J. Chem. Phys. **102**, 8138 (1995).
10. M.J. Uttormark, M.O. Thompson, and P. Clancy, Phys. Rev. B **47**, 15717 (1993).
11. C.J. Tymczak and J.R. Ray, J. Chem. Phys. **92**, 7520 (1990).
12. F. Celestini and J.M. Debierre, Phys. Rev. E **65**, 041605 (2002).
13. J.Q. Broughton and G.H. Gilmer, J. Chem. Phys. **84**, 5759 (1986).
14. R.L. Davidchack and B.B. Laird, Phys. Rev. Lett. **85**, 4751 (2000).
15. J.J. Hoyt, M. Asta, and A. Karma, Phys. Rev. Lett. **86**, 5530 (2001).
16. J.R. Morris, S.Y. Lu, and K.M. Ho, Interface Science (current issue).
17. M.S. Daw and M.I. Baskes, Phys. Rev. Lett. **50**, 1285 (1983); Phys. Rev. B **29**, 6443 (1984).
18. R. Ravelo and M.I. Baskes, MRS Symp. Proc. **398** (1996).
19. H.E.A. Huitema, B. van Hengstum, and J.P. van der Eerden, J. Chem. Phys. **111**, 10248 (1999).
20. Q.M. Yu, M.O. Thompson, and P. Clancy, Phys. Rev. B **53**, 8386 (1996).
21. F. Celestini and J.M. Debierre, Phys. Rev. B **62**, 14006 (2000).
22. R.L. Davidchack and B.B. Laird, Phys. Rev. E **54**, R5905 (1996); Mol. Phys. **97**, 833 (1999).
23. R. Sibug-Aga and B.B. Laird, J. Chem. Phys. **116**, 3410 (2002).
24. T. Akamatsu and K. Kawamura, Mol. Simul. **21**, 387 (1999).

25. S.M. Foiles, Phys. Rev. B **32**, 7685 (1985).
26. C.H.P. Lupis, *Chemical Thermodynamics of Materials* (Elsevier, New York, 1983).
27. M. Asta and S.M. Foiles, Phys. Rev. B **53**, 2389 (1996).
28. S.M. Foiles, Phys. Rev. B **40**, 11502 (1989).
29. S.M. Foiles, Mater. Res. Soc. Symp. Proc. **63**, 61 (1985).
30. R.W. Smith, R. Najafabadi, and D.J. Srolovitz, Acta Metall. Mater. **43**, 3621 (1995).
31. J.R. Morris, C.Z. Wang, K.M. Ho, and C.T. Chan, Phys. Rev. B **49**, 3109 (1994).
32. *Binary Alloy Phase Diagrams*, 2nd edn., edited by T.B. Massalski, H. Okamoto, P.R. Subramanian, and L. Kacprzak (ASM International, Materials Park, OH, 1990).
33. M. Asta, D. Morgan, J.J. Hoyt, B. Sadigh, J.D. Althoff, D. de Fontaine, and S.M. Foiles, Phys. Rev. B **59**, 14271 (1999).
34. *Selected Values of Thermodynamic Properties of Metals and Alloys*, edited by R.R. Hultgren, P.D. Anderson, and K.K. Kelly (Wiley, New York, 1963).
35. D.A. Shashkov, M.F. Chisholm, and D.N. Seidman, Acta Mater. **47**, 3939 (1999); D.A. Shaskov, D.A. Muller, and D.N. Seidman, Acta Mater. **47**, 3953 (1999).
36. J. Rusing, J.T. Sebastian, O.C. Helman, and D.N. Seidman, Microsc. Microanal. **6**, 445 (2000).
37. S.A. Dregia and P. Wynblatt, Acta Metall. Mater. **39**, 771 (1991).
38. C. Huang, M. Overa de la Cruz, and P.W. Voorhees, Acta Mater. **47**, 4449 (1999).
39. A. Umantsev, Phys. Rev. B **64**, 075419 (2001).